A Synoptic View of the Third Uniform California Earthquake Rupture Forecast (UCERF3)

by Edward H. Field, Thomas H. Jordan, Morgan T. Page, Kevin R. Milner, Bruce E. Shaw, Timothy E. Dawson, Glenn P. Biasi, Tom Parsons, Jeanne L. Hardebeck, Andrew J. Michael, Ray J. Weldon II, Peter M. Powers, Kaj M. Johnson, Yuehua Zeng, Karen R. Felzer, Nicholas van der Elst, Christopher Madden, Ramon Arrowsmith, Maximilian J. Werner, and Wayne R. Thatcher

ABSTRACT

Probabilistic forecasting of earthquake-producing fault ruptures informs all major decisions aimed at reducing seismic risk and improving earthquake resilience. Earthquake forecasting models rely on two scales of hazard evolution: long-term (decades to centuries) probabilities of fault rupture, constrained by stress renewal statistics, and short-term (hours to years) probabilities of distributed seismicity, constrained by earthquake-clustering statistics. Comprehensive datasets on both hazard scales have been integrated into the Uniform California Earthquake Rupture Forecast, Version 3 (UCERF3). UCERF3 is the first model to provide self-consistent rupture probabilities over forecasting intervals from less than an hour to more than a century, and it is the first capable of evaluating the short-term hazards that result from multievent sequences of complex faulting. This article gives an overview of UCERF3, illustrates the short-term probabilities with aftershock scenarios, and draws some valuable scientific conclusions from the modeling results. In particular, seismic, geologic, and geodetic data, when combined in the UCERF3 framework, reject two types of fault-based models: long-term forecasts constrained to have local Gutenberg–Richter scaling, and short-term forecasts that lack stress relaxation by elastic rebound.

INTRODUCTION

More than a century of searching has failed to identify diagnostic precursory signals that can reliably predict the occurrence of large earthquakes (Jordan *et al.*, 2011). However, observed seismic activity can constrain the probabilities of future earthquakes at two scales of hazard evolution—the short-term decay of aftershocks caused by abrupt stress perturbations during rupture (e.g., Reasenberg and Jones, 1989), and the long-term delay needed to reload fault stress after elastic rebound (e.g., Working Group on California Earthquake Probabilities [WGCEP], 1988). Consistent modeling across both scales of stress evolution is a key requirement for operational earthquake forecasting in seismically active regions (Jordan *et al.*, 2011). The societal need for such models has been underscored by the extensive damage and loss of life caused by multievent sequences in Japan, New Zealand, and Italy during the last year alone.

The tectonic reloading of stress by steady block motion, originally postulated by H. F. Reid in his elastic rebound theory (Reid, 1911) and later explained by plate tectonics, was the basis for a series of fault-specific rupture forecasts developed by WGCEP (1988, 2003). California's San Andreas fault system releases most of the plate-boundary strain in strike-slip earthquakes with moment magnitudes M greater than 7.5 and recurrence intervals of a century or more. WGCEP has represented successive large ruptures of a fault using a renewal process with a distribution of interevent times calibrated against historical and paleoseismic data and the date of the last event, where it is known, to condition the probability of the next event.

The preceding WGCEP model, Uniform California Earthquake Rupture Forecast, Version 2 (UCERF2), restricted fault-slip events to full ruptures of predefined fault segments and some contiguous combinations (Field *et al.*, 2009). Moreover, it generally excluded the possibility of ruptures jumping from one fault to another nearby fault, a phenomenon observed in California and other highly interconnected fault systems (e.g., Wesnousky, 2006). UCERF2 also overpredicted the rate of $6.5 \le M \le 7.0$ earthquakes relative to historical seismicity. This intermediate-magnitude bulge was reduced relative to previous California models (Frankel *et al.*, 2002), but a discrepancy remained, which WGCEP hypothesized to be an artifact of the segmentation assumptions restricting multifault ruptures (Field *et al.*, 2009).

A different class of models, based on aftershock statistics, has been developed to assess short-term changes in seismic hazard. Examples include the Reasenberg–Jones model (Reasenberg

doi: 10.1785/0220170045

and Jones, 1989, 1994), the short-term earthquake probability (STEP) model (Gerstenberger *et al.*, 2005), and the epidemic-type aftershock sequence (ETAS) model (Ogata, 1988; Helmstetter and Sornette, 2002). Earthquake activity is represented as a stochastic point process that obeys the observed power-law scaling of aftershock excitation with mainshock size and aftershock decay in space and time (Omori–Utsu statistics). Each event is marked by a moment magnitude M independently drawn from a fixed magnitude–frequency distribution (MFD), usually in the Gutenberg–Richter (GR) form: $\log N = a - bM$, in which N is the expected number of events and $b \approx 1$. STEP uses the Reasenberg–Jones model to forecast average aftershock rates from preidentified mainshocks, whereas ETAS models aftershocks via Monte Carlo simulations, in which every earthquake is a mainshock with its own aftershocks, explicitly accounting for multiple generations of triggered seismicity (epidemics). In both types of models, aftershocks can be larger than the mainshock.

These aftershock models ignore proximity to known faults when specifying the probability of a large earthquake being triggered. In addition, aftershock decay and stress-renewal delay exhibit opposing statistical behaviors with conflicting hazard implications. According to Omori–Utsu clustering, the most likely place for the next event is the location of the most recent one; according to Reid renewal, the least likely fault to rupture is the one that ruptured most recently. Omori–Utsu sequences of aftershocks are more clustered than a Poisson process, whereas Reid sequences of elastic rebounds are more periodic. The new forecasting framework represented in Uniform California Earthquake Rupture Forecast, Version 3 (UCERF3) merges these opposing behaviors into a consistent multiscale model by conditioning the short-term ETAS forecast on the long-term Reid forecast.

UNIFORM CALIFORNIA EARTHQUAKE RUPTURE FORECAST, VERSION 3 (UCERF3)

The model comprises three levels of forecasting: a time-independent model, UCERF3-TI (Field *et al.*, 2014); a long-term time-dependent refinement based on Reid-renewal statistics, UCERF3-TD (Field *et al.*, 2015); and a short-term clustering model based on ETAS statistics, UCERF3-ETAS (Field *et al.*, 2017). The model is hierarchical in the sense that the TD probabilities are conditioned on the TI model, and the ETAS probabilities are conditioned on the TD model (Fig. 1).

UCERF3-TI gives the long-term rates of all earthquakes with $M \geq 2.5$ throughout the California region. Target earthquakes are of two types: supraseismogenic ruptures on modeled faults with $M \geq M_{ss}$, in which M_{ss} is the minimum magnitude of a rupture spanning the seismogenic layer, and gridded seismicity from MFDs assigned on a $0.1° \times 0.1°$ geographic mesh. All faults were divided into small subsections with along-strike lengths of about half the down-dip width, typically ~7 km (Fig. 1a). Fault-based ruptures were defined by sets of two or more contiguous subsections, corresponding to $M_{ss} \approx 6.3$. We omitted ruptures that jumped fault gaps exceeding 5 km, a value consistent with the limited observations (Wesnousky, 2006) and supported by rupture simulations (e.g., Harris *et al.*, 1991), and we excluded those that failed a stress-compatibility test. The number of fault-based ruptures in UCERF3 is ~250, 000 compared with ~8000 in UCERF2. The magnitude of each rupture was computed from empirical scaling relations that relate moment magnitude to rupture area.

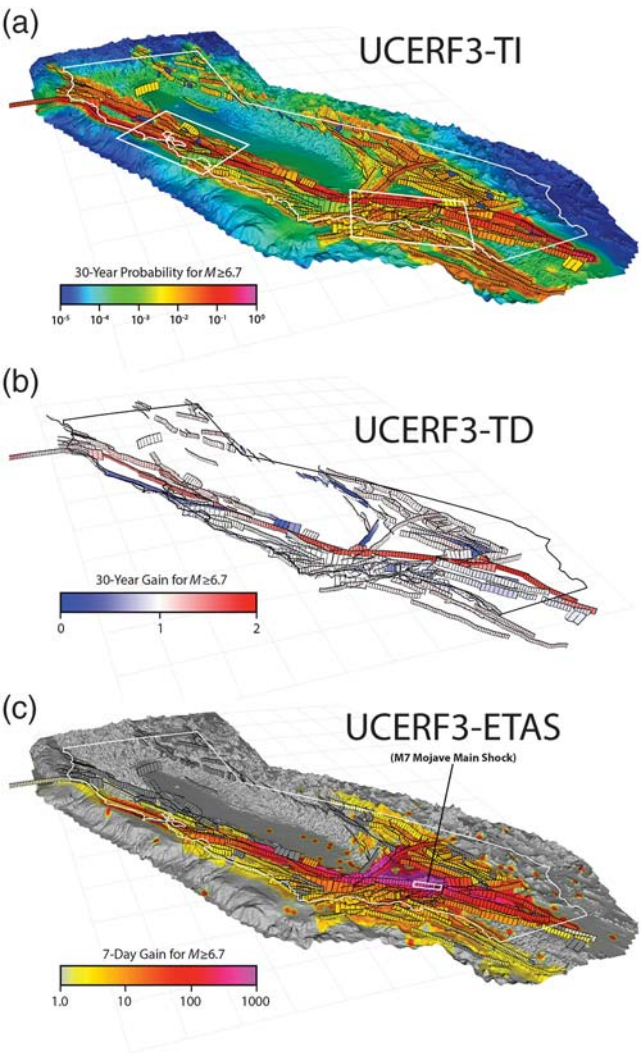

▲ **Figure 1.** (a) Time-independent (TI) probabilities that certain locations in greater California will participate in one or more $M \geq 6.7$ earthquake ruptures during a 30 year interval. Modeled fault subsections are depicted as black-outlined parallelograms. (b) Time-dependent (TD) participation probability gains relative to TI for $M \geq 6.7$ fault ruptures during the next 30 year interval. (c) Epidemic-type aftershock sequence (ETAS) probability gains relative to TI for $M \geq 6.7$ earthquakes during a 7 day interval immediately following an M 7 scenario on the Mojave section of the San Andreas fault. Mainshock rupture area is outlined in white.

A system-wide grand inversion simultaneously determined the rates of all ruptures by minimizing a quadratic objective function measuring the model's misfit to fault-slip rates, paleoseismic event rates, and observed seismicity. This underdetermined problem was regularized by smoothness conditions and

solved by simulated annealing under appropriate positivity constraints (Page *et al.*, 2014). The inversion approach was less prescriptive than previous methodologies; for example, it determined the range of MFDs most consistent with available data, rather than assuming a functional form. As expected, relaxing fault segmentation and allowing multifault ruptures eliminated the intermediate-magnitude overprediction (bulge) evident in UCERF2; the consequent transfer of moment release to larger magnitudes increased the 30-year statewide probability of an $M \geq 8$ earthquake from 4.7% to 7.0%. Other improvements included a revised, more extensive model of active California faults and the inclusion of kinematically consistent deformation models that assimilated both geodetic and geologic data in estimating fault-slip rates (Parsons *et al.*, 2013). UCERF3-TI implies that about two-thirds of deformation not attributed to defined faults goes into permanent strain not described by purely elastic behavior.

The model was evaluated by applying quantitative and visual measures of its fit to independent data subsets, which were then assessed by expert panels. Expert opinion was also elicited in weighting the 1440 branches of the logic tree used to represent the UCERF3-TI epistemic uncertainties. The hazard obtained by combining the UCERF3-TI model with ground-motion prediction equations has been incorporated into the 2014 revisions of the National Seismic Hazard Maps (Petersen *et al.*, 2014).

UCERF3-TD was built by augmenting UCERF3-TI with a composite Reid renewal model that conditioned the rupture probabilities on the open interval, defined as the time since a fault subsection last participated in a supraseismogenic event. In UCERF2, the renewal model could be enforced at the fault-segment level, and the probabilities were balanced to approximate slip rates on a fault-by-fault basis (Field *et al.*, 2009). To relax segmentation and include multifault ruptures, it was necessary to enforce the UCERF3 renewal statistics at the fault-subsection level and to balance the probabilities at the fault system level. This was accomplished by a system-wide averaging algorithm that accounted for the variability of the recurrence and open intervals among the fault subsections involved in a specified rupture. On many faults, the date of the last supraseismogenic event is unknown. It is unlikely, however, that such events could have occurred in California without detection after 1875; hence, a 140-year historic open interval was used as a lower bound on the date of last event, allowing time-dependent probabilities to be cast for all fault-based ruptures. The renewal model also incorporated magnitude-dependent aperiodicity factors that adjusted the interevent times of smaller events to be more variable than those of larger ones. Epistemic uncertainties were represented by four levels of temporal predictability specified by aperiodicity factors of a Brownian passage time model (WGCEP, 2003) ranging from 0.4 to 1.0.

Compared with the TI model, TD probabilities are relatively low on faults where a large event has recently occurred and relatively high where the time since last event exceeds the average recurrence interval (Fig. 1b). Places where the rupture probabilities are high compared to the TI model include the San Andreas fault in southern California and the Hayward–Rodgers Creek fault in northern California, which both show probability gains of about a factor of two.

UCERF3-ETAS represents spatiotemporal clustering, including aftershocks and other triggered earthquake activity, discretized onto an ~2 km mesh. The forecasting statistics for an interval $0 < t \leq T$ are computed from large sets of $M \geq 2.5$ catalogs simulated within the TD framework. Each simulation is initialized at $t = 0$ with an observed or hypothetical $M \geq 2.5$ catalog of past earthquakes. Every earthquake, observed or simulated, is allowed to trigger a set of first-generation aftershocks by using Monte Carlo sampling from an ETAS model that has spatial and temporal kernels calibrated to California seismicity (Hardebeck, 2013); they in turn trigger second-generation aftershocks and so on for all subsequent generations up to time T. Earthquakes that occur spontaneously according to UCERF3-TD probabilities, typically ~30% of the total, also trigger aftershocks.

In UCERF3-ETAS, the probabilities of all fault-based supraseismogenic ruptures, including aftershocks, are conditioned by Reid renewal statistics that evolve during the seismic sequence; that is, the probability of a fault subsection participating in a future event is reduced if that subsection has already participated in a previous event of the sequence. The explicit inclusion of elastic rebound in modeling earthquake sequences is essential to the stability of the UCERF3-ETAS model, as discussed below.

The probabilities of large aftershocks ($M \geq 6.7$) in the week following a scenario M 7 rupture of the Mojave section of the San Andreas fault are mapped in Figure 1c as probability gains relative to UCERF3-TD. Relatively high gains (up to ~100) extend spatially along nearby faults—not only the high-rate San Andreas, but also low-rate faults such as the Cucamonga and Garlock.

A wide variety of metrics for forecasting hazard and loss can be derived from the UCERF3-ETAS model, including the likelihood of large earthquakes during multievent sequences of complex faulting. The number of Monte Carlo simulations needed to obtain stable forecast estimates depends on the metric of interest. Estimates in this article were derived from ensembles of 10^4 to 4×10^5 catalogs.

Figure 2 shows the UCERF3-ETAS aftershock forecast following an M 6.1 earthquake on the Parkfield section of the San Andreas fault and compares it with an equivalent one from an ETAS model that lacks faults. Aftershock nucleation in the former extends along the major faults of the San Andreas system, unlike the smooth isotropic distribution forecast by the ETAS point-process model. This scenario is particularly interesting because an M 6.1 foreshock is known to have occurred near Parkfield about two hours before the 1857 Fort Tejon earthquake, an M 7.8 rupture that propagated down the San Andreas from Parkfield to Cajon Pass (Sieh, 1978; Meltzner and Wald, 1999). According to UCERF3-ETAS, in the first week following the M 6.1 initial event, the average probability of an $M \geq 7.8$ rupture extending southeastward along

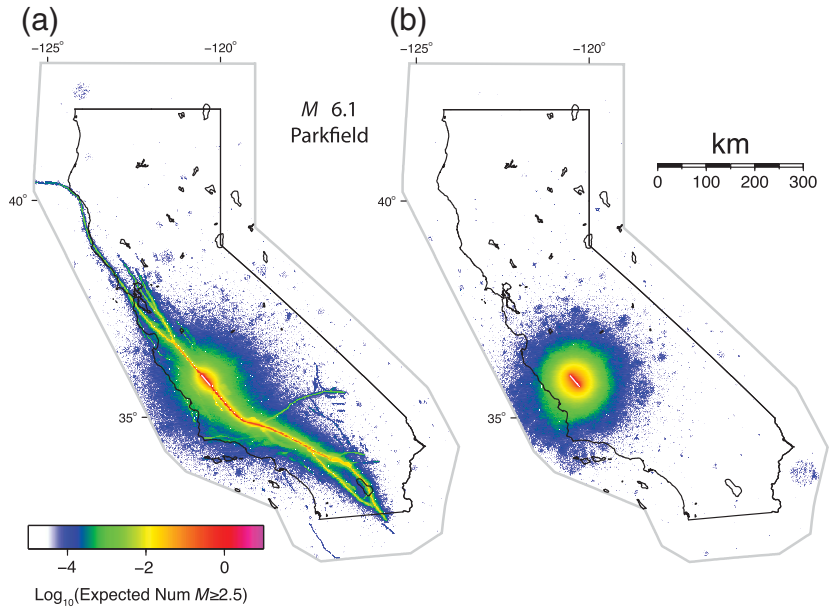

▲ **Figure 2.** (a) Aftershock nucleation rates following an M 6.1 earthquake on the Parkfield section of the San Andreas fault, based on 2×10^5 Uniform California Earthquake Rupture Forecast, Version 3 (UCERF3)-ETAS simulations. The map shows the average number of $M \geq 2.5$ earthquakes nucleating in 0.02° × 0.02° cells over a 7 day period immediately following the mainshock rupture, which is plotted as a white line. (b) Aftershock nucleation rates following the same M 6.1 mainshock computed from an equivalent ETAS model with no faults.

the San Andreas to the Mojave South section is 5.8×10^{-3}. In contrast, the probability of an $M \geq 7.8$ rupture extending northwestward through the creeping section to the Peninsula section is 4.0×10^{-4}, more than an order of magnitude lower. The isotropic probability of an $M \geq 7.8$ aftershock from the no-fault ETAS model is 1.2×10^{-3}.

The hierarchical UCERF3 model is complex, and its substantial epistemic uncertainties have yet to be fully investigated. We can nevertheless identify two types of forecasting models within the UCERF3 framework that are rejected by the UCERF3 datasets and modeling assumptions: long-term models with local GR scaling and short-term models without stress relaxation (elastic rebound).

INADEQUACY OF LOCAL GR SCALING

Below some outer scale M_{max}, the total seismicity of a region as large as northern or southern California can be well described by a GR-MFD with a b-value near unity (Felzer, 2013). There has been considerable debate, however, about whether a GR-MFD applies in small regions of high-rate faulting (Ishibe and Shimazaki, 2012; Kagan *et al.*, 2012; Page *et al.*, 2015). An alternative is the characteristic MFD hypothesis, which states that the rate of supraseismogenic ruptures on major faults such as the San Andreas is elevated above the GR extrapolation of the small-magnitude seismicity (Youngs and Coppersmith, 1985).

We tested these competing hypotheses by inverting the earthquake-rate data with and without local GR-MFD constraints. Unconstrained inversions obtain acceptable models in which the MFDs of some faults are characteristic while others are anticharacteristic; that is, depleted in large earthquakes relative to the GR extrapolation (e.g., Fig. 3a). This behavior can be measured by a characteristic factor C_M defined as the cumulative rate of ruptures above some supraseismogenic magnitude $M \geq M_{ss}$, here taken to be 7.0, divided by the extrapolated GR rate. The empirical distribution of C_7 across all subsections has a mean value of 2.18 and a standard deviation of 2.21. More subsections are strongly characteristic (37% with $C_7 > 2.0$) than strongly anticharacteristic (20% with $C_7 < 0.5$). The C_7 values show a positive correlation with moment release; weighting subsections by their moment rates increases the C_7 mean to 3.20. No model with a narrow distribution of C_7 about unity, as required by the local GR hypothesis, produced acceptable fits to the observed fault-slip rates and regional event rates (Field *et al.*, 2014).

The UCERF3-TI dataset thus strongly favors the characteristic MFD hypothesis over the local GR hypothesis. The model corrects for the aseismic creep rate measured locally across faults (Weldon *et al.*, 2013), as well as the aseismic deformation derived from the geodetic and geologic modeling (Parsons *et al.*, 2013). The corrected slip rates require, on average, significantly higher rates of large earthquakes than predicted by local GR scaling. Explaining the discrepancy in terms of aseismic slip would require a 50% reduction in the average seismic slip rate or a 50% overprediction of the regional seismicity rates. The former was rejected as a viable alternative by the UCERF3 expert review panel (Field *et al.*, 2014); the latter was rejected by a one-sided test against the empirical MFD for California at the 97.5% confidence level (Felzer, 2013).

In Figure 3, we compare aftershocks that occurred in the week following an M 4.8 mainshock near the southern end of the Coachella section of the San Andreas fault (characteristic MFD, $C_7 = 5.8$) with those from an M 4.8 mainshock on the Borrego segment of the San Jacinto fault (anticharacteristic MFD, $C_7 = 0.25$). The corresponding probabilities that these events will trigger one or more $M \geq 7.0$ aftershocks are 1.7×10^{-3} and 7.4×10^{-5}, respectively, compared to a GR probability of 3.3×10^{-4}. The probability gains relative to GR, 5.1 and 0.22, directly reflect the characteristic factors. In general, the magnitude distribution of short-term aftershocks from a small mainshock near an active fault is governed by that fault's long-term magnitude probability distribution (Michael, 2012).

For both examples in Figure 3, the UCERF3-TD characteristic factors deviate from unity by more than the UCERF3-TI characteristic factors ($C_7 = 2.1$ and 0.41), illustrating the

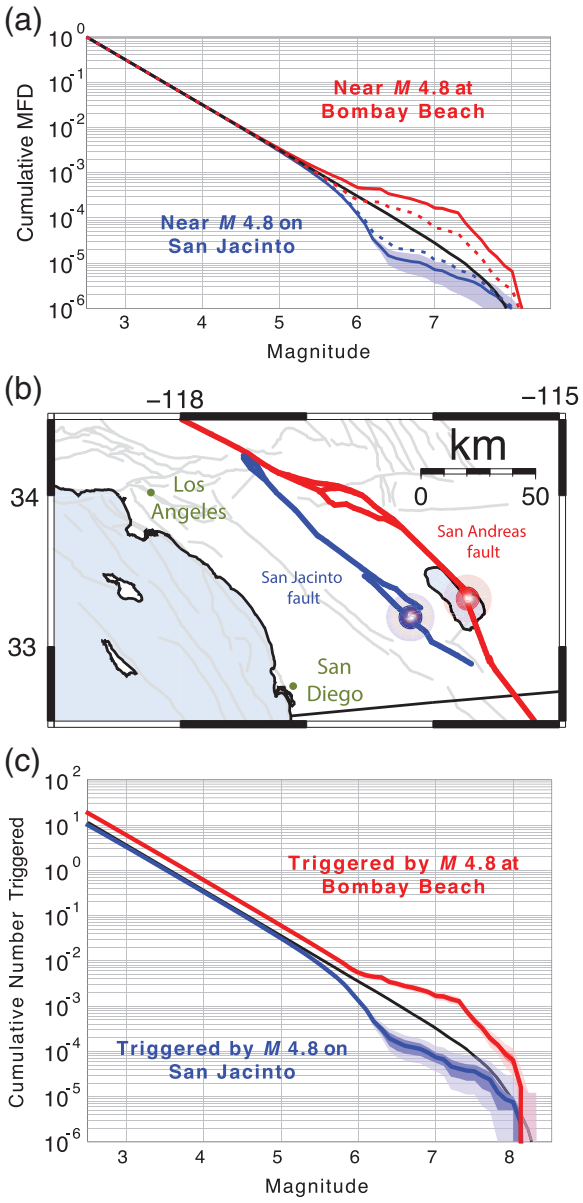

▲ **Figure 3.** (a) Cumulative long-term magnitude–frequency distributions (MFDs) for a point near the Coachella section of the San Andreas fault (red) and the Borrego section of the San Jacinto fault (blue), compared with the regional Gutenberg–Richter (GR) distribution (black). Distributions for the mean TI model (dotted) and mean TD model (solid) are averages of the nearby MFDs weighted by the spatial ETAS kernels centered on the events shown in (b). Shaded bands represent the modeling uncertainties. (b) Faults (color lines) and locations of the *M* 4.8 mainshock scenarios (red and blue circles). The Coachella hypocenter is offset about 4 km from the fault terminus to mimic the 24 March 2009 Bombay Beach event. (c) Expected number of aftershocks forecast during the first week following the *M* 4.8 Coachella and Borrego scenarios (red and blue lines, respectively), compared to the regional GR model (black line). The dark and light shaded bounds represent modeling and sampling uncertainties, respectively; the latter are from a Wilson score interval with continuity correction (Newcombe, 1998).

direct effect of the long-term renewal model on the short-term probabilities. For the Coachella section, where the last large earthquake occurred over 300 years ago, the gain is significant even at small magnitudes; that is, the one-week probability of one or more $M \geq 4.8$ aftershocks is 0.091, compared with the standard GR value of 0.05 often used as a seismological rule of thumb (Reasenberg and Jones, 1994).

THE NEED FOR ELASTIC REBOUND

The applicability of elastic rebound in earthquake forecasting remains controversial (Kagan *et al.*, 2012; Tormann *et al.*, 2015; Bürgmann *et al.*, 2016; Mulargia *et al.*, 2016). In UCERF3-TD, elastic rebound is modeled as a Reid renewal process in which rupture of a fault subsection instantaneously reduces the probability of that subsection participating in a future rupture. If we do not include this elastic rebound in UCERF3-ETAS, the model does not produce realistic earthquake sequences. The ETAS probability density of triggering a new rupture increases with proximity to an old rupture; hence, without a renewal mechanism for lowering the rupture probability, the subsection most likely to rupture is one that has just ruptured. Sequences are then dominated by recurring re-ruptures of the same fault area, which is not observed in nature (Field *et al.*, 2017). Motivated by earlier assertions of this issue (Field, 2011), van der Elst and Shaw (2015) subsequently found that aftershocks larger than the mainshock tend to nucleate in the outer regions of the parent aftershock zone, which they interpreted as the inhibition of re-rupturing by stress relaxation.

In UCERF3 simulations, elastic rebound is required to inhibit re-ruptures of faults with characteristic factors as low as unity (i.e., with GR-MFDs). Moreover, aftershock sequences near faults with even moderately characteristic MFDs can become unstable without it. The calibration of ETAS parameters by Hardebeck (2013) using regional California earthquake catalogs yields an effective branching ratio near its critical value of unity; on average, each event eventually spawns about one other event over infinite time, which implies that almost all events are triggered and very few are spontaneous. When these regional statistics are applied in the vicinity of faults with high-characteristic factors, the local branching ratio exceeds unity, and the sequences exhibit explosive exponential growth. The application of elastic rebound tames this unrealistic growth by lowering the characteristic factor after a rupture.

Figure 4 illustrates the average one-week aftershock nucleation frequencies in the Los Angeles region following an *M* 7.0 scenario on the Mojave section of the San Andreas fault and in the San Francisco region for an *M* 7.1 scenario on the Hayward fault. The former is the same as in Figure 1c, and the latter is similar to the scenario used by the U.S. Geological Survey in its HayWired preparedness study (Detweiler and Wein, 2017). The aftershock distributions are again extended along the major faults. The aftershock MFDs show immediate probability gains of two orders of magnitude or more relative

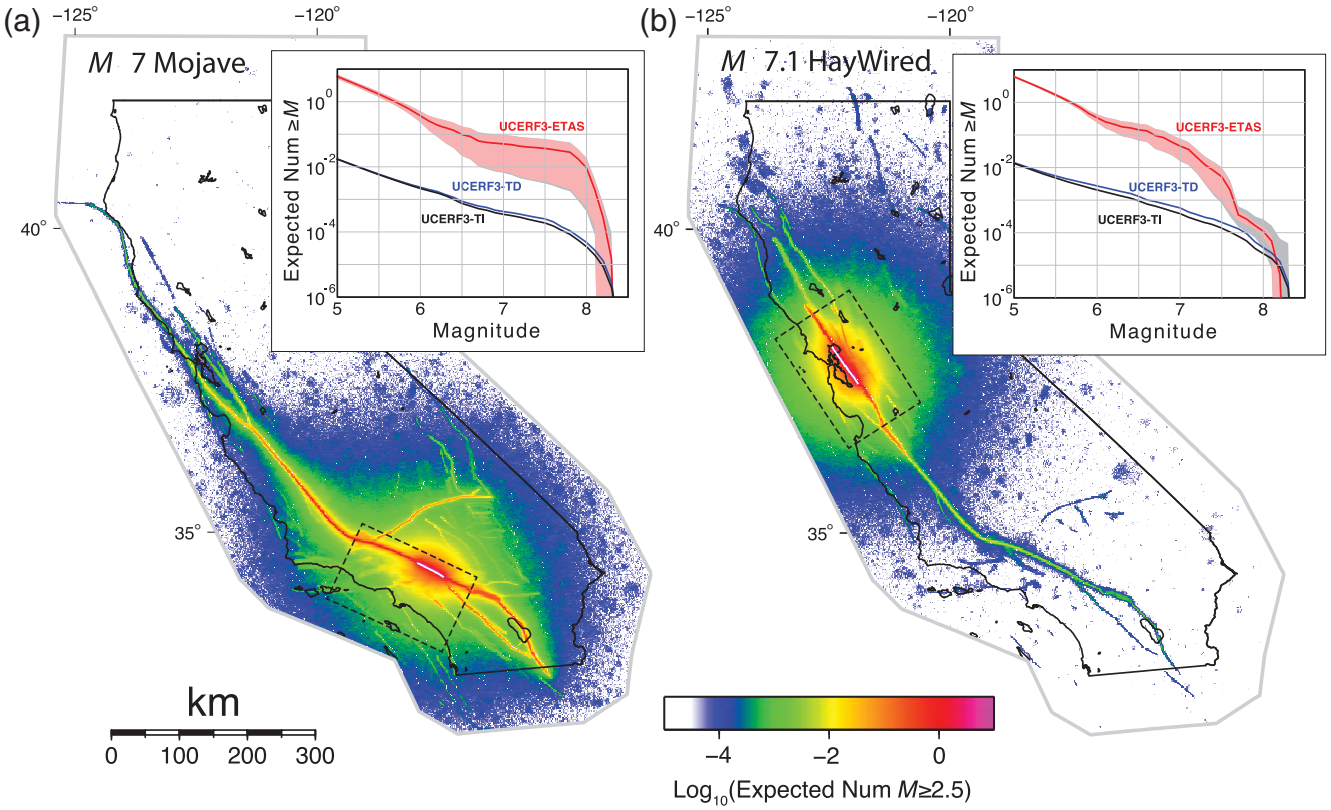

▲ **Figure 4.** (a) Aftershock nucleation rates following an M 7 earthquake on the Mojave section of the San Andreas fault based on 2×10^5 UCERF3-ETAS simulations. The map shows the average number of $M \geq 2.5$ earthquakes nucleating in 0.02° × 0.02° cells over a 7 day period immediately following the mainshock (white line). (Inset) MFD for ruptures with some part inside the dashed box defining the greater Los Angeles area. The red line is the average 7 day aftershock MFD, where the red shading represents the modeling uncertainty and the gray shading represents sampling uncertainty. Corresponding 7 day MFDs for UCERF3-TI and UCERF3-TD are in black and blue lines, respectively. (b) Same as (a), but for an M 7.1 mainshock on the Hayward fault; inset graph pertains to the dashed box defining the San Francisco Bay area.

to UCERF3-TD, and their shape differences reflect the characteristic factors and open intervals of the nearby faults.

Figure 4 also illustrates the influence of one important uncertainty—the extent to which smaller aftershocks occurring on the mainshock rupture surface can trigger large fault ruptures. The darker colored bands in Figures 3 and 4 show the range bracketed by the two end-member hypotheses (triggering allowed, or not). The difference can be up to an order of magnitude for the M 7 Mojave scenario. Limited observations suggest that such triggering is suppressed on recently ruptured faults (van der Elst and Shaw, 2015), but the evidence is far from conclusive with respect to larger ruptures. We have, therefore, equally weighted these two possibilities to obtain the mean values (solid lines) in Figures 3 and 4.

DISCUSSION

The hierarchical and modular structure of UCERF3 provides a self-consistent framework for earthquake forecasting across the complete range of temporal and spatial scales, from aftershocks during the first hours following small spatially distributed events to the largest earthquakes expected on the San Andreas fault system over intervals of many decades. Relaxation of fault segmentation and allowance of multifault ruptures substantially increases the complexity and multiplicity of possible ruptures, reducing the characteristic factors near faults and improving agreement with observed seismicity.

Previous fault-based models have not included aftershocks and other manifestations of earthquake clustering, and ETAS point-process models have not accounted for known faults or stress relaxation during rupture. The novel coupling of Omori–Utsu clustering statistics to Reid renewal statistics permits the estimation of earthquake triggering probabilities conditioned by the proximity of events to active faults, and the resulting model is capable of representing the short-term hazards due to multievent sequences of complex faulting. The model can be updated with observed seismicity to capture the static or dynamic triggering effects that play out during a particular sequence. The multiscale framework is adaptable to many other continental fault systems, and the short-term component might be applicable to the forecasting of induced seismicity.

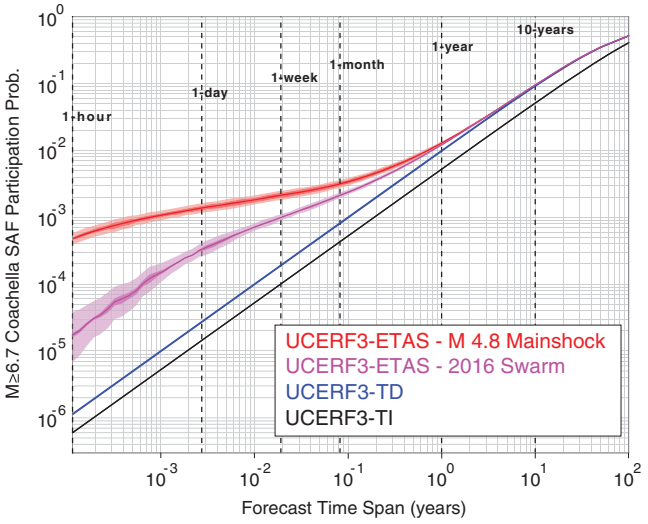

▲ **Figure 5.** Probability of one or more $M \geq 6.7$ earthquakes on the Coachella section of the San Andreas fault versus forecast time span for UCERF3-TI (black line) and UCERF3-TD (blue line). UCERF3-ETAS probabilities following the M 4.8 Bombay Beach event of Figure 2 are shown in red, and those following a 2016 swarm are shown in magenta. The latter start time is at 08:30 (local time) on 27 September 2016.

The UCERF3 project has augmented and refined the seismic, geologic, and geodetic constraints on California earthquake activity. When consistently combined within the UCERF3 modeling framework, these datasets reject long-term forecasts constrained to have local Gutenberg–Richter scaling and short-term forecasts that lack stress relaxation by elastic rebound. One or both of these model-based inferences could be wrong, of course, but a Type-I error at this high level would likely require basic revisions to our most fundamental assumptions regarding seismic energy release in plate-boundary deformation zones.

UCERF3 is under evaluation by the U.S. Geological Survey as a prototype component of an operational earthquake forecasting system (Field *et al.*, 2016). The proposed validation steps include prospective testing of UCERF3 in the Collaboratory for the Study of Earthquake Predictability (Zechar *et al.*, 2010), evaluation of its consistency with earthquake sequences observed in similar tectonic environments, and comparison of its forecasts with those derived from physics-based earthquake simulators. Figure 5 shows an example application to the southeastern end of the San Andreas fault, where the occurrence of small earthquakes in 2009 and 2016 prompted alerts by the California Office of Emergency Services (Jordan and Jones, 2010). The UCERF3-ETAS probability gains decay rapidly, dropping from two orders of magnitude in the first hour to one order of magnitude over the first week for the 2009 event, which raises the question of model valuation. Earthquake forecasts possess no intrinsic societal value; rather, they acquire value through their ability to influence decisions made by the public and decision-makers seeking to mitigate seismic risk (Jordan *et al.*, 2011). The value of the UCERF3 short-term forecasts will need to be ascertained in the context of specific applications.

DATA AND RESOURCES

All simulation data presented in this article are available at http://www.WGCEP.org/UCERF3-ETAS (last accessed March 2017) and all calculations were made using OpenSHA (http://www.OpenSHA.org, last accessed March 2017), which in turn utilizes Generic Mapping Tools (http://gmt.soest.hawaii.edu, last accessed January 2012) and JFreeChart (http://www.jfree.org/jfreechart/, last accessed March 2012) for making plots.

ACKNOWLEDGMENTS

The Uniform California Earthquake Rupture Forecast, Version 3 (UCERF3) development was supported by the California Earthquake Authority, U.S. Geological Survey (USGS), USGS- Southern California Earthquake Center (SCEC) Cooperative Agreement G12AC20038, and National Science Foundation (NSF)-SCEC Cooperative Agreement EAR-1033462. Calculations were performed at the Texas Advanced Computing Center and the USC Center for High-Performance Computing and Communications. We thank the USGS Powell Center for Analysis and Synthesis for supporting workshops on UCERF3-epidemic-type aftershock sequence (ETAS) development, and the W. M. Keck Foundation for supporting the integration of UCERF3 into the Collaboratory for Interseismic Modeling and Simulation. We also thank Michael Blanpied, Matt Gerstenberger, and an anonymous individual for constructive review comments. The SCEC Contribution Number for this article is 7165.

REFERENCES

Bürgmann, R., N. Uchide, Y. Hu, and T. Matsuzawa (2016). Tohoku rupture reloaded? *Nat. Geosci.* **9,** 183–184.

Detweiler, S. T., and A. M. Wein (Editors) (2017). The HayWired earthquake scenario—Earthquake hazards, *U.S. Geol. Surv. Scientific Investig. Rept. 2017-5013-A–H*, 126 pp., doi: 10.3133/sir20175013v1.

Felzer, K. R. (2013). Appendix K: The UCERF3 earthquake catalog, *U.S. Geol. Surv. Open-File Rept. 2013-1165-K* and *California Geol. Surv. Special Rept. 228-K*.

Field, E. H. (2011). Aftershock statistics constitute the strongest evidence for elastic rebound in large earthquakes, presented at the *2011 Fall Meeting, AGU*, San Francisco, California, 5–9 December, Abstract S22B–08.

Field, E. H., R. J. Arrowsmith, G. P. Biasi, P. Bird, T. E. Dawson, K. R. Felzer, D. D. Jackson, K. M. Johnson, T. H. Jordan, C. Madden, *et al.* (2014). Uniform California Earthquake Rupture Forecast, version 3 (UCERF3)—The time-independent model, *Bull. Seismol. Soc. Am.* **104,** 1122–1180, doi: 10.1785/0120130164.

Field, E. H., R. J. Arrowsmith, G. P. Biasi, P. Bird, T. E. Dawson, K. R. Felzer, D. D. Jackson, K. M. Johnson, T. H. Jordan, C. Madden, *et al.* (2015). Long-term, time-dependent probabilities for the Third Uniform California Earthquake Rupture Forecast (UCERF3), *Bull. Seismol. Soc. Am.* **105,** 511–543, doi: 10.1785/0120140093.

Field, E. H., T. E. Dawson, K. R. Felzer, A. D. Frankel, V. Gupta, T. H. Jordan, T. Parsons, M. D. Petersen, R. S. Stein, R. J. Weldon II, *et al.*

(2009). Uniform California Earthquake Rupture Forecast, Version 2 (UCERF 2), *Bull. Seismol. Soc. Am.* **99,** 2053–2107, doi: 10.1785/0120080049.

Field, E. H., T. H. Jordan, L. M. Jones, A. J. Michael, M. L. Blanpied, and Other Workshop Participants (2016). The potential uses of operational earthquake forecasting, *Seismol. Res. Lett.* **80,** 1–10, doi: 10.1785/0220150174.

Field, E. H., K. R. Milner, J. L. Hardebeck, M. T. Page, N. van der Elst, T. H. Jordan, A. J. Michael, B. E. Shaw, and M. J. Werner (2017). A spatiotemporal clustering model for the Third Uniform California Earthquake Rupture Forecast (UCERF3-ETAS): Toward an operational earthquake forecast, *Bull. Seismol. Soc. Am.* **107,** doi: 10.1785/0120160173.

Frankel, A. D., M. D. Petersen, C. S. Mueller, K. M. Haller, R. L. Wheeler, E. V. Leyendecker, R. L. Wesson, S. C. Harmsen, C. H. Cramer, D. M. Perkins, *et al.* (2002). Documentation for the 2002 update of the national seismic hazard map, *U.S. Geol. Surv. Open-File Rept. 2002-420*.

Gerstenberger, M., S. Wiemer, L. M. Jones, and P. A. Reasenberg (2005). Real-time forecasts of tomorrow's earthquakes in California, *Nature* **435,** 328–331.

Hardebeck, J. L. (2013). Appendix S: Constraining epidemic type aftershock sequence (ETAS) parameters from the Uniform California Earthquake Rupture Forecast, Version 3 catalog and validating the ETAS model for magnitude 6.5 or greater earthquakes, *U.S. Geol. Surv. Open-File Rept. 2013-1165-S* and *California Geol. Surv. Special Rept. 228-S*.

Harris, R. A., R. J. Archuleta, and S. M. Day (1991). Fault steps and the dynamic rupture process: 2D numerical simulations of a spontaneously propagating shear fracture, *Geophys. Res. Lett.* **18,** 893–896.

Helmstetter, A., and D. Sornette (2002). Sub-critical and supercritical regimes in epidemic models of earthquake aftershocks, *J. Geophys. Res.* **107,** 2237.

Ishibe, T., and K. Shimazaki (2012). Characteristic earthquake model and seismicity around late Quaternary active faults in Japan, *Bull. Seismol. Soc. Am.* **102,** 1041–1058.

Jordan, T. H., and L. M. Jones (2010). Operational earthquake forecasting: Some thoughts on why and how, *Seismol. Res. Lett.* **81,** no. 4, 571–574.

Jordan, T. H., Y.-T. Chen, P. Gasparini, R. Madariaga, I. Main, W. Marzocchi, G. Papadopoulos, G. Sobolev, K. Yamaoka, and J. Zschau (2011). Operational earthquake forecasting: State of knowledge and guidelines for implementation, final report of the International Commission on Earthquake Forecasting for Civil Protection, *Ann. Geophys.* **54,** no. 4, 315–391, doi: 10.4401/ag-5350.

Kagan, Y. Y., D. D. Jackson, and R. J. Geller (2012). Characteristic earthquake model, 1884-2011, R.I.P., *Seismol. Res. Lett.* **83,** 951–953, doi: 10.1785/0220120107.

Meltzner, A. J., and D. J. Wald (1999), Foreshocks and aftershocks of the great 1857 California earthquake, *Bull. Seismol. Soc. Am.* **89,** 1109–1120.

Michael, A. J. (2012). Fundamental questions of earthquake statistics and estimation of earthquake probabilities from possible foreshocks, *Bull. Seismol. Soc. Am.* **102,** 2547–2562, doi: 10.1785/0120090184.

Mulargia, F., P. B. Stark, and R. J. Geller (2016). Why is probabilistic seismic hazard analysis (PSHA) still used? *Phys. Earth Planet. In.* **264,** 63–75, doi: 10.1016/j.pepi.2016.12.002.

Newcombe, R. G. (1998). Two-sided confidence intervals for the single proportion: Comparison of seven methods, *Stat. Med.* **17,** 857–872.

Ogata, Y. (1988). Statistical models of point occurrences and residual analysis for point processes, *J. Am. Stat. Assoc.* **83,** 9–27.

Page, M. T., and K. R. Felzer (2015). Southern San Andreas fault seismicity is consistent with the Gutenberg–Richter magnitude–frequency distribution, *Bull. Seismol. Soc. Am.* **105,** no. 4, doi: 10.1785/0120140340.

Page, M. T., E. H. Field, K. R. Milner, and P. M. Powers (2014). The UCERF3 grand inversion: Solving for the long-term rate of ruptures in a fault system, *Bull. Seismol. Soc. Am.* **104,** 1181–1204, doi: 10.1785/0120130180.

Parsons, T., K. M. Johnson, P. Bird, J. M. Bormann, T. E. Dawson, E. H. Field, W. C. Hammond, T. A. Herring, R. McCaffrey, Z.-K. Shen, *et al.* (2013). Appendix C: Deformation models for UCERF3.3, *U.S. Geol. Surv. Open-File Rept. 2013-1165-C* and *California Geol. Surv. Special Rept. 228-C*.

Petersen, M. D., M. P. Moschetti, P. M. Powers, C. S. Mueller, K. M. Haller, A. D. Frankel, Y. Zeng, S. Rezaeian, S. C. Harmsen, and O. S. Boyd (2014). Documentation for the 2014 update of the United States National Seismic Hazard maps, *U.S. Geol. Surv. Open-File Rept. 2014-1091*, 243 pp., doi: 10.3133/ofr20141091

Reasenberg, P., and L. Jones (1994). Earthquake aftershocks: Update, *Science* **265,** 1251–1252.

Reasenberg, P. A., and L. M. Jones (1989). Earthquake hazard after a mainshock in California, *Science* **243,** 1173–1176.

Reid, H. F. (1911). The elastic-rebound theory of earthquakes, *Univ. Calif. Pub. Bull. Dept. Geol. Sci.* **6,** 413–444.

Sieh, K. E. (1978). Central California foreshocks of the great 1857 earthquake, *Bull. Seismol. Soc. Am.* **68,** 1731–1749.

Tormann, T., B. Enescu, J. Woessner, and S. Wiemer (2015). Randomness of megathrust earthquakes implied by rapid stress recovery after the Japan earthquake, *Nat. Geosci.* **8,** 152–158.

van der Elst, N. J., and B. E. Shaw (2015). Larger aftershocks happen farther away: Nonseparability of magnitude and spatial distributions of aftershocks, *Geophys. Res. Lett.* **42,** 5771–5778, doi: 10.1002/2015GL064734.

Weldon, R. J., II, D. A. Schmidt, L. J. Austin, E. M. Weldon, and T. E. Dawson (2013). Appendix D: Compilation of creep rate data for California faults and calculation of moment reduction due to creep, *U.S. Geol. Surv. Open-File Rept. 2013-1165-S* and *California Geol. Surv. Special Rept. 228-S*.

Wesnousky, S. G. (2006). Predicting the endpoints of earthquake futures, *Nature* **444,** 358–360, doi: 10.1038/nature05275.

Working Group on California Earthquake Probabilities (WGCEP) (1988). Probabilities of large earthquakes occurring in California on the San Andreas fault, *U.S. Geol. Surv. Open-File Rept. 88-398*, 62 pp.

Working Group on California Earthquake Probabilities (2003). Earthquake probabilities in the San Francisco Bay region: 2002–2031, *U.S. Geol. Surv. Open-File Rept. 2003-214*.

Youngs, R. R., and K. J. Coppersmith (1985). Implications of fault slip rates and earthquake recurrence models to probabilistic seismic hazard estimates, *Bull. Seismol. Soc. Am.* **75,** 939–964.

Zechar, J. D., D. Schorlemmer, M. Liukis, J. Yu, F. Euchner, P. J. Maechling, and T. H. Jordan (2010). The Collaboratory for the Study of Earthquake Predictability perspectives on computational earth science, *Concurr. Comput. Pract. Exper.* **22,** 1836–1847, doi: 10.1002/cpe.1519.

Edward H. Field
Peter M. Powers
Yuehua Zeng
U.S. Geological Survey
Denver Federal Center
P.O. Box 25046, MS-966
Denver, Colorado 80225-0046 U.S.A.
field@usgs.gov

Thomas H. Jordan
Kevin R. Milner
University of Southern California
Southern California Earthquake Center
3651 Trousdale Parkway Number 169
Los Angeles, California 90089-0742 U.S.A.

Morgan T. Page
Karen R. Felzer
Nicholas van der Elst
U.S. Geological Survey
525 S. Wilson Avenue
Pasadena, California 91106 U.S.A.

Bruce E. Shaw
Lamont Doherty Earth Observatory
Columbia University
Palisades, New York 10964 U.S.A.

Timothy E. Dawson
California Geological Survey
345 Middlefield Road, MS-520
Menlo Park, California 94025 U.S.A.

Glenn P. Biasi
University of Nevada Reno
Nevada Seismological Laboratory
1664 N. Virginia Street, MS-174
Reno, Nevada 89557 U.S.A.

Tom Parsons
U.S. Geological Survey
345 Middlefield Road, MS-999
Menlo Park, California 94025 U.S.A.

Jeanne L. Hardebeck
Andrew J. Michael
Wayne R. Thatcher
U.S. Geological Survey
345 Middlefield Road, MS-977
Menlo Park, California 94025 U.S.A.

Ray J. Weldon II
Department of Earth Sciences
University of Oregon
Eugene, Oregon 97403-1272 U.S.A.

Kaj M. Johnson
Department of Geological Sciences
Indiana University
1001 E. 10th Street
Bloomington, Indiana 47405 U.S.A.

Christopher Madden
College of Earth, Ocean, and Atmospheric Sciences
Oregon State University
104 CEOAS Administration Building
Corvallis, Oregon 97331-5503 U.S.A.

Ramon Arrowsmith
School of Earth and Space Exploration
Arizona State University
P.O. Box 876004
Tempe, Arizona 85287-6004 U.S.A.

Maximilian J. Werner
School of Earth Sciences and Cabot Institute
University of Bristol
Wills Memorial Building, Queen's Road
Bristol BS8 1RJ, United Kingdom

Published Online 12 July 2017